

## INFLAMMATORY BOWEL DISEASE

## Epithelial OPA1 links mitochondrial fusion to inflammatory bowel disease

Li-Li Bao<sup>1</sup>, Yu-Qiang Yu<sup>1†</sup>, Miguel González-Acera<sup>1</sup>, Jay V. Patankar<sup>1</sup>, Andreas Giessl<sup>2</sup>, Gregor Sturm<sup>3</sup>, Anja A. Kühl<sup>4,5</sup>, Raja Atreya<sup>1,6</sup>, Lena Erkert<sup>1</sup>, Reyes Gámez-Belmonte<sup>1</sup>, Susanne M. Krug<sup>4</sup>, Benjamin Schmid<sup>7</sup>, Philipp Tripal<sup>7</sup>, Mircea T. Chiriac<sup>1</sup>, Kai Hildner<sup>1,6</sup>, Britta Siegmund<sup>4</sup>, Stefan Wirtz<sup>1</sup>, Michael Stürzl<sup>8</sup>, Mariam Mohamed Abdou<sup>8</sup>, Zlatko Trajanoski<sup>3</sup>, TRR241 IBDome Consortium‡, Markus F. Neurath<sup>1,6</sup>, Antonio Zorzano<sup>9,10,11</sup>, Christoph Becker<sup>1,6\*</sup>

Copyright © 2025 The Authors, some rights reserved; exclusive licensee American Association for the Advancement of Science. No claim to original U.S. Government Works

Dysregulation at the intestinal epithelial barrier is a driver of inflammatory bowel disease (IBD). However, the molecular mechanisms of barrier failure are not well understood. Here, we demonstrate dysregulated mitochondrial fusion in intestinal epithelial cells (IECs) of patients with IBD and show that impaired fusion is sufficient to drive chronic intestinal inflammation. We found reduced expression of mitochondrial fusion-related genes, such as the dynamin-related guanosine triphosphatase (GTPase) optic atrophy 1 (*OPA1*), and fragmented mitochondrial networks in crypt IECs of patients with IBD. Mice with *Opa1* deficiency in the gut epithelium (*Opa1*<sup>iMEC</sup>) spontaneously developed chronic intestinal inflammation with mucosal ulcerations and immune cell infiltration. Intestinal inflammation in *Opa1*<sup>iMEC</sup> mice was driven by microbial translocation and associated with epithelial progenitor cell death and gut barrier dysfunction. *Opa1*-deficient epithelial cells and human organoids exposed to a pharmacological OPA1 inhibitor showed disruption of the mitochondrial network with mitochondrial fragmentation and changes in mitochondrial size, ultrastructure, and function, resembling changes observed in patient samples. Pharmacological inhibition of the GTPase dynamin-1-like protein in organoids derived from *Opa1*<sup>iMEC</sup> mice partially reverted this phenotype. Together, our data demonstrate a role for epithelial OPA1 in regulating intestinal immune homeostasis and epithelial barrier function. Our data provide a mechanistic explanation for the observed mitochondrial dysfunction in IBD and identify mitochondrial fusion as a potential therapeutic target in this disease.

## INTRODUCTION

Inflammatory bowel disease (IBD) describes chronic inflammatory conditions that affect the gut, with the two primary forms being Crohn's disease (CD) and ulcerative colitis (UC). The cause of IBD is not well understood, and curative therapies are lacking. IBD is believed to have a multifactorial etiology involving microbiota-driven immune responses and dysregulation of epithelial homeostasis leading to a compromised gut barrier (1). Intestinal epithelial cells (IECs) constitute a physical barrier, separating the contents of

the gut from the underlying tissues. In addition, specialized IECs secrete mucus, antimicrobial peptides, and cytokines, exerting innate immune functions to further enhance gut tissue defense. Functional studies in mice have provided direct evidence that the intestinal epithelium is a critical component in preventing IBD and that dysregulation of epithelial homeostasis can cause loss of gut immune tolerance (1).

Mitochondrial dysfunction has been suggested as a feature of IBD (2–6). For example, reduced adenosine triphosphate (ATP) has been reported in the intestines of patients with IBD (6). Moreover, enterocytes isolated from patients with IBD exhibit mitochondria with altered structure and irregular cristae (2–4, 7). Several studies have revealed an involvement of mitochondrial stress in IBD, with altered mitochondrial health implicated by gene expression studies in CD and UC cohorts (8, 9). Circulating mitochondrial DNA (mtDNA), a pro-inflammatory mediator, was released during active disease in patients with CD and UC (10). In addition, induction of the mitochondrial unfolded protein response has been demonstrated in epithelial cells of patients with CD and UC (9, 11). Given these observations, IBD has been suggested to be associated with mitochondrial dysfunction. However, what causes mitochondrial dysfunction in IBD is not fully known.

Mitochondria form a highly dynamic network within eukaryotic cells and constantly undergo changes in their morphology because of the processes of fusion and fission, a remnant of their endosymbiotic evolutionary origin (12). Whereas fission is a process by which mitochondria segregate into two separate organelles, mitochondrial fusion can merge two or more mitochondria into one (12). Tight control of mitochondrial dynamics is considered

<sup>1</sup>Department of Medicine 1, Friedrich-Alexander-Universität Erlangen-Nürnberg (FAU) and Universitätsklinikum Erlangen, 91052 Erlangen, Germany. <sup>2</sup>Department of Ophthalmology, Friedrich-Alexander-Universität Erlangen-Nürnberg (FAU) and Universitätsklinikum Erlangen, 91054 Erlangen, Germany. <sup>3</sup>Biocenter, Institute of Bioinformatics, Medical University of Innsbruck, 6020 Innsbruck, Austria. <sup>4</sup>Medizinische Klinik für Gastroenterologie, Infektiologie und Rheumatologie, Charité-Universitätsmedizin Berlin, corporate member of Freie Universität Berlin and Humboldt-Universität zu Berlin, 10117 Berlin, Germany. <sup>5</sup>iPATH.Berlin, Charité-Universitätsmedizin Berlin, corporate member of Freie Universität Berlin and Humboldt Universität zu Berlin, 10117 Berlin, Germany. <sup>6</sup>Deutsches Zentrum Immuntherapie (DZI), 91054 Erlangen, Germany. <sup>7</sup>Optical Imaging Centre Erlangen (OICE), Friedrich-Alexander-Universität Erlangen-Nürnberg (FAU), 91058 Erlangen, Germany. <sup>8</sup>Division of Molecular and Experimental Surgery, Department of Surgery, Friedrich-Alexander-Universität (FAU) Erlangen-Nürnberg and Universitätsklinikum Erlangen, 91054 Erlangen, Germany. <sup>9</sup>Institute for Research in Biomedicine (IRB Barcelona), Barcelona Institute of Science and Technology, 08028 Barcelona, Spain. <sup>10</sup>Departament de Bioquímica i Biomedicina Molecular, Facultat de Biologia, Universitat de Barcelona, 08028 Barcelona, Spain. <sup>11</sup>Centro de Investigación Biomédica en Red de Diabetes y Enfermedades Metabólicas Asociadas (CIBERDEM), Instituto de Salud Carlos III, 28029 Madrid, Spain.

\*Corresponding author. Email: christoph.becker@uk-erlangen.de

†Present address: Department of Cardiology, Second Affiliated Hospital, School of Medicine, Zhejiang University, Hangzhou 310009, China.

‡Contributing authors and their affiliations are listed at the end of the Acknowledgments.

key to mitochondrial quality control, particularly during cellular stress (12, 13). Pathophysiological alterations in mitochondrial fission and fusion have recently been implicated in neurodegenerative diseases and cancer (14–16). Moreover, recent findings suggest an involvement of dysregulated mitochondrial dynamics in inflammatory processes (17, 18). Mitochondrial fusion has been reported to promote cell survival given that fusion of a dysfunctional mitochondrion with an intact mitochondrion can serve as a repair process that preserves the mitochondrial network (19). Mitochondrial fusion is driven by OPA1, a dynamin-related mitochondrial guanosine triphosphatase (GTPase) together with Mitofusin-1 (MFN1) and Mitofusin-2 (MFN2) (12, 13). In this study, we investigated the gut tissues of patients with IBD and mice lacking *Opa1* in the intestinal epithelium to evaluate the hypothesis that dysregulated mitochondrial dynamics might drive intestinal inflammation and contribute to the pathophysiology of IBD.

## RESULTS

### Mitochondrial dysfunction in patients with IBD is associated with mitochondrial fragmentation and diminished expression of the fusion regulators OPA1, MFN1, and MFN2

To analyze mitochondria in patients with IBD, we analyzed endoscopic biopsies with active inflammation using transmission electron microscopy (TEM). Particularly in the colons of patients with UC and in the lower crypt region of the small intestines in patients with CD, we observed IECs with mitochondrial abnormalities as indicated by less electron-dense mitochondria with disrupted cristae structure as compared with control individuals without intestinal inflammation (Fig. 1A and fig. S1A). Moreover, whereas IECs in uninflamed samples from control individuals showed a dense mitochondrial network with elongated and branched mitochondria, IECs in inflamed samples from patients with IBD showed a fragmented network and fewer elongated and branched mitochondria (Fig. 1A and fig. S1B). Of note, elongated and branched mitochondria have been described as indicators of mitochondrial fusion events (20), suggesting impaired mitochondrial dynamics in epithelial cells of patients with IBD. Consistent with this observation, we noted a decreased expression of mitochondrial genes and proteins in gut samples from patients with CD or UC (Fig. 1B; fig. S1, C and D; and tables S1 and S2). These data from our own cohorts were supported by a reanalysis of transcriptomic data from a publicly available UC dataset (PROTECT cohort), which also showed a lower expression of mitochondrial genes in patient samples than in controls (fig. S1E), confirming previous analyses (21). The expression of several of these genes was negatively correlated with the degree of histological inflammation, suggesting that dysregulation of mitochondria is associated with inflammatory stress (fig. S1F).

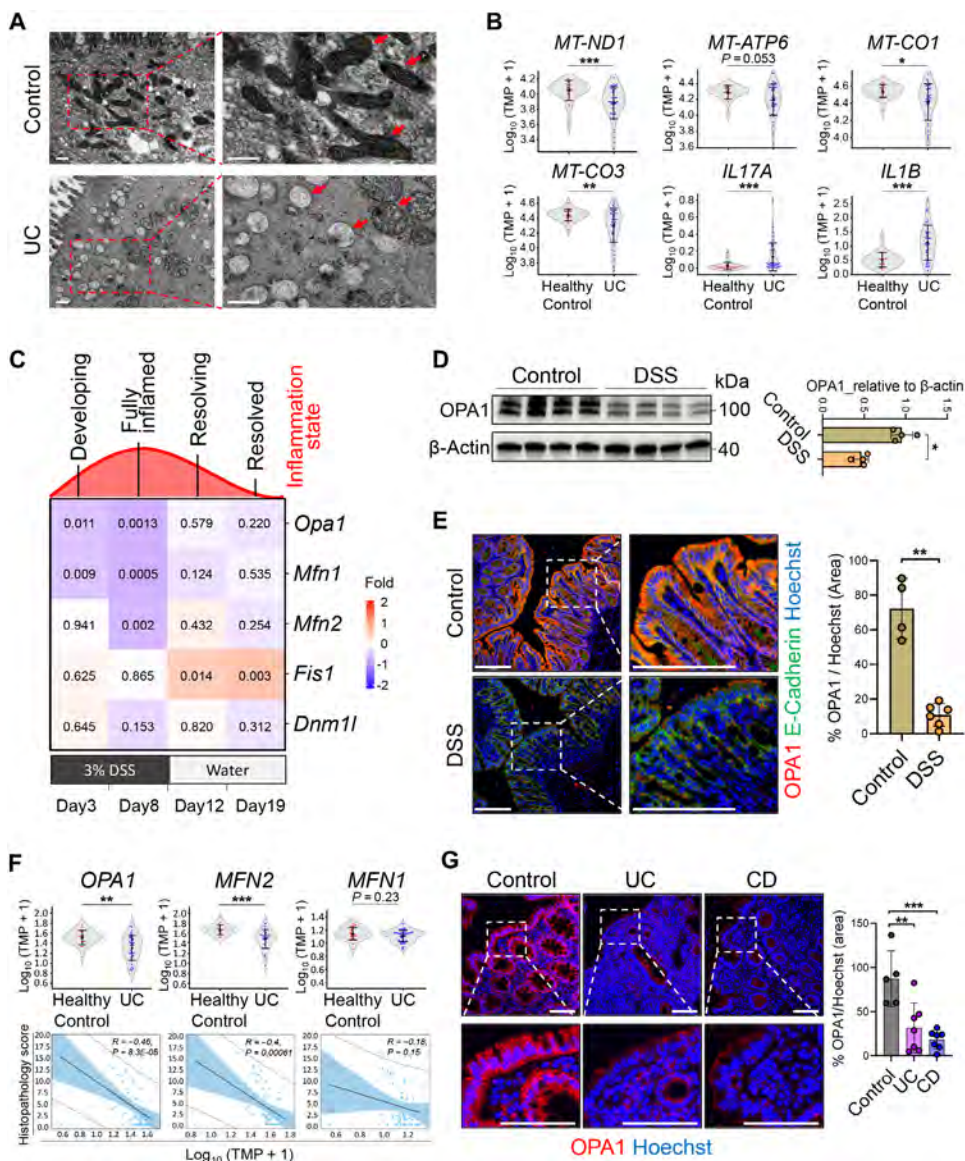
To further investigate the involvement of mitochondrial dynamics in the pathophysiology of intestinal inflammation, we performed a time-course experiment of dextran sodium sulfate (DSS)-induced colitis in mice and performed RNA sequencing (RNA-seq) at different time points during the development and resolution of experimental colitis to compare the expression of key mitochondrial genes. We observed a significant down-regulation of *Opa1* ( $P = 0.0013$ ), *Mfn1* ( $P = 0.0005$ ), and *Mfn2* ( $P = 0.002$ ),

the key regulators of mitochondrial fusion, at the peak of experimental colitis (Fig. 1C). Of note, expression of the mitochondrial fission molecule *Fis1* ( $P = 0.003$ ) was significantly increased during the resolution phase, suggesting a dynamic regulation of mitochondrial fission and fusion during the course of colitis. *Opa1* ( $P = 0.011$ ) and *Mfn1* ( $P = 0.009$ ) were significantly down-regulated already at the onset of colitis development, suggesting a role for these molecules early in the pathophysiology of intestinal inflammation. The down-regulation of OPA1 during experimental colitis was further confirmed by Western blotting of colon tissue lysates of mice with acute DSS-induced colitis (Fig. 1D). Diminished expression of OPA1 was particularly evident in the intestinal epithelium as demonstrated by immunohistochemical staining of tissue sections from the inflamed colons of mice subjected to either DSS colitis (Fig. 1E) or four other well-established models of acute and chronic colitis in mice (fig. S2A). On the basis of these findings, we speculated that mitochondrial fusion in IECs is impaired in intestinal inflammation.

To compare our findings of colitis-dependent suppression of mitochondrial fusion-related genes in mice (Fig. 1C) with tissues from patients with IBS, we next analyzed the expression of OPA1, MFN1, and MFN2 as critical molecules for mitochondrial fusion in our cohort of patients with UC. Similarly to our data from experimental colitis, we found that OPA1 ( $P = 0.00166$ ) and MFN2 ( $P = 2.383 \times 10^{-5}$ ) were significantly down-regulated in patients compared with controls (Fig. 1F). To substantiate our findings in an independent cohort and to stratify for OPA1 expression in different cell types, we analyzed publicly available single-cell RNA-seq data from a cohort of patients with UC and control individuals (22) to examine the expression of OPA1, MFN1, and MFN2 in different cellular compartments and disease stages. Consistently with our own dataset, all three genes were decreased in the epithelial compartment of inflamed gut samples when compared with noninflamed patient samples and when compared with healthy controls (fig. S2B). In the immune compartment, all three genes were increased in inflamed gut samples (fig. S2C), suggesting that the lower epithelial expression of OPA1, MFN1, and MFN2 is cell-type specific. Similarly, in our own set of tissues from patients with IBD, we noted a reduction in OPA1 and MFN2 during active inflammation, with amounts higher in patients in remission (fig. S2, D to F). Moreover, the expression of OPA1 ( $P = 8.3 \times 10^{-5}$ ) and MFN2 ( $P = 0.00061$ ) showed a significant negative correlation to histological scores of inflammation (Fig. 1F) and to the expression of IBD-relevant inflammation markers (fig. S3), again suggesting that inflammatory stress in the gut is associated with a down-regulation of mitochondrial fusion in these patients. Down-regulation of OPA1 mRNA expression was also observed in our cohort of patients with CD (fig. S2, E and F), along with negative correlations to inflammation markers (fig. S3), although not to the extent observed in UC. Down-regulation of epithelial OPA1 protein was also evident in immunohistochemical staining for OPA1 in control versus both CD and UC colon samples (Fig. 1G). Thus, our findings in patients with IBD and in mice with experimental colitis suggest that mitochondrial dysfunction in IBD might be caused by dysregulated mitochondrial dynamics in IECs and that impaired mitochondrial fusion in IECs might be a driver of gut inflammation and a cause of mitochondrialopathy.

**Fig. 1. Dysregulated mitochondrial dynamics in patients with IBD.**

**(A)** Representative TEM images of mitochondria in biopsies from the sigmoid colons of control individuals and patients with UC ( $n = 3$  or 4 per group). Arrows indicate mitochondria. Scale bars, 500 nm. **(B)** Expression of the mitochondrial and pro-inflammatory genes in bulk transcriptomic data of colonic biopsies from 22 control individuals and 45 patients with UC. **(C)** Heatmap showing differential expression of mitochondrial dynamics-related genes during the course of DSS-induced colitis and recovery in wild-type mice relative to untreated control mice. Mice were euthanized at day 3, 8, 12, or 19. Colors depict  $\log_2$ -fold change (red, up; blue, down), and numbers indicate adjusted  $P$  values. **(D)** Representative immunoblot of OPA1 in colon samples (left) and quantification (right) from control mice and from mice treated with 3% DSS for 6 days.  $\beta$ -Actin was used as a control ( $n = 4$ ). **(E)** Representative images (left) and quantification (right) of immunostaining for OPA1 (red) and E-cadherin (green) in colon tissues from control mice and mice treated with DSS ( $n = 4$  to 6). Nuclei were stained with Hoechst 33342 (blue). Scale bars, 128  $\mu$ m. **(F)** Expression of *OPA1*, *MFN1*, and *MFN2* in colonic samples of healthy control individuals versus patients with UC (top) and in correlation with the respective histopathological score of colitis ( $n = 22$  control and 45 patients with UC) (bottom). **(G)** Representative images of OPA1-stained (red) control and UC and CD colon samples ( $n = 5$  to 7 per group). Nuclei were stained with Hoechst 33342 (blue). Scale bars, 128  $\mu$ m. \* $P < 0.05$ ; \*\* $P < 0.01$ ; \*\*\* $P < 0.001$ ; Mann-Whitney test [(B), (D), (E), and (F)] or two-way ANOVA with Tukey's correction (G). Data are means  $\pm$  SD.

**Mice with *Opa1* deficiency in IECs spontaneously develop gut inflammation with histological features similar to patients with IBD**

To investigate the impact of impaired mitochondrial fusion and the consequence of reduced *Opa1* expression in the intestinal epithelium, we crossed mice carrying loxP-flanked *Opa1* alleles (*Opa1<sup>loxP/loxP</sup>*) with *Villin-CreERT2* transgenic mice, resulting in mice (*Opa1<sup>iΔIEC</sup>*) in which *Opa1* could be deleted specifically in the intestinal epithelium at any time by injection of tamoxifen. IEC-specific ablation of *Opa1* expression after tamoxifen injection in *Opa1<sup>iΔIEC</sup>* mice was confirmed by immunohistochemistry (IHC) (Fig. 2A) and by quantitative polymerase chain reaction (qPCR) and Western blotting of either whole colonic tissue (fig. S4A) or pure IEC cultures (fig. S4B). In contrast with control mice, *Opa1<sup>iΔIEC</sup>* mice began to lose weight within 2 weeks of *Opa1* deletion and continued to do so until termination criteria (according to animal ethics) were reached (Fig. 2B). High-resolution endoscopy of *Opa1<sup>iΔIEC</sup>* mice revealed signs of

colitis, including bowel wall thickening, mucosal erosions, increased granularity, and colonic mucosal bleeding (Fig. 2C). Spontaneous gut inflammation was further supported by in vivo imaging of inflammation (fig. S4C), reduced gut length (fig. S4D), and enlarged mesenteric lymph nodes (fig. S4E) in *Opa1<sup>iΔIEC</sup>* mice. Histological analysis revealed marked destruction of the gut architecture and evidence of severe inflammation in the ilea, ceca, and colons of *Opa1<sup>iΔIEC</sup>* mice, with bowel wall thickening, increased cellularity, and crypt erosion in all *Opa1<sup>iΔIEC</sup>* mice analyzed (Fig. 2D). Our finding of spontaneous intestinal inflammation in mice lacking *Opa1* in IECs was further supported by massive infiltration of the lamina propriae of *Opa1<sup>iΔIEC</sup>* mice with MPO<sup>+</sup> neutrophils, F4/80<sup>+</sup> macrophages, and CD4<sup>+</sup> T cells (Fig. 2E) and by increased expression of inflammatory mediators, such as *S100a9*, *Nos2*, *Tnf*, *Il1β*, *Ifit1*, and *Cxcl10*, in these animals (Fig. 2F). Microbiome changes are a common feature of IBD when compared with healthy individuals (23). Of note, 16S-based metabarcoding analysis demonstrated no

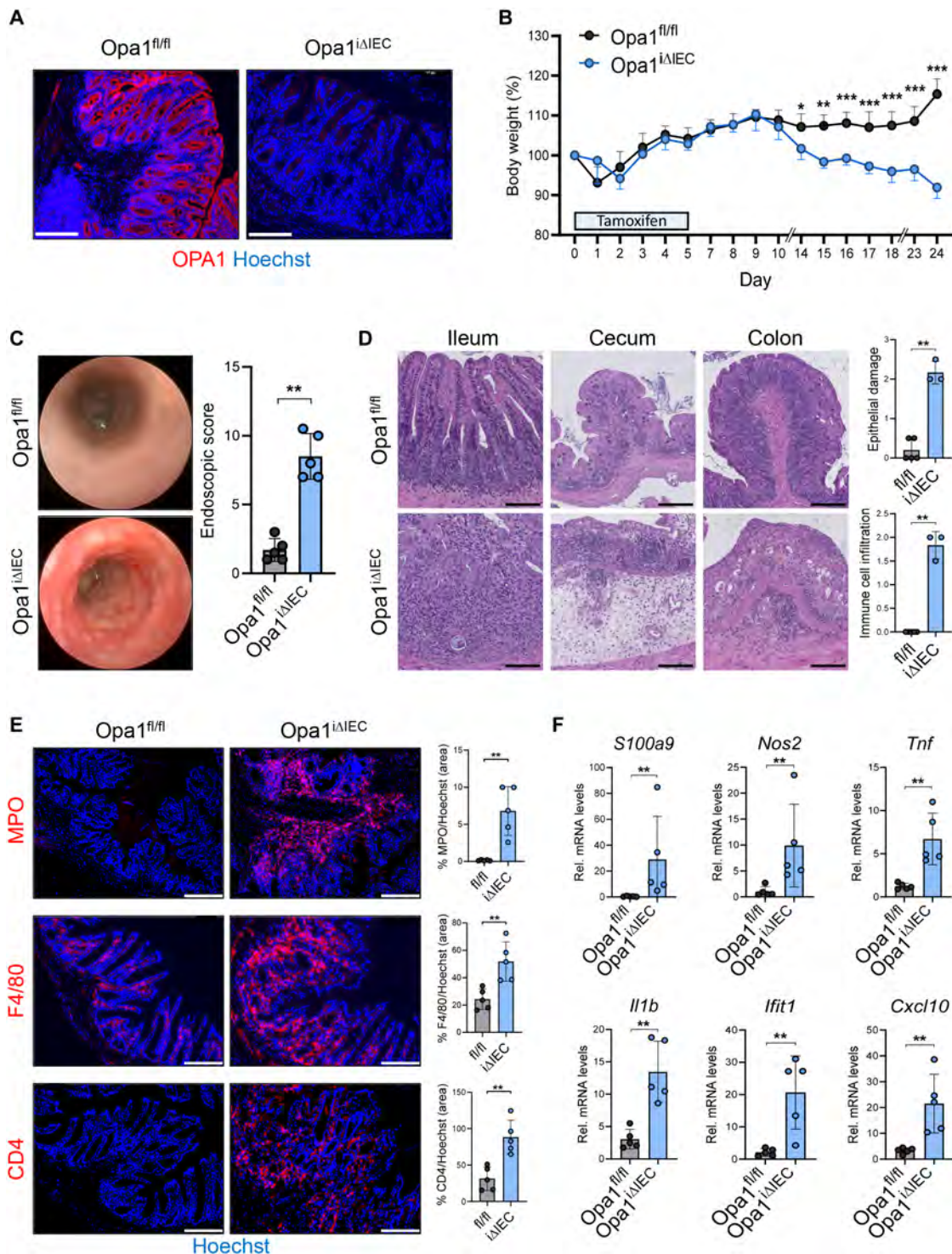


**Fig. 2. Intestinal epithelium-specific *Opa1* ablation causes severe chronic ileocolitis.** (A) OPA1 immunostaining (red) of colon sections from control and *Opa1*<sup>ΔIEC</sup> mice (*n* = 5). Nuclei were counterstained with Hoechst 33342 (blue). Scale bars, 128 μm. (B) Relative body weight of *Opa1*<sup>fl/fl</sup> and *Opa1*<sup>ΔIEC</sup> mice after 5 days of tamoxifen administration, monitored over time and shown as percentage (%) of initial weight (*n* = 3 to 5 per group; data expressed as means ± SD). (C) Representative endoscopic images of the colon (left) and MEICS endoscopic score (right) of *Opa1*<sup>fl/fl</sup> and *Opa1*<sup>ΔIEC</sup> mice 24 days after tamoxifen administration (*n* = 5; data expressed as means ± SD). (D) Representative histological images of H&E staining (left) and histological scores (right) representing epithelial damage (0 to 3 score range) and immune cell infiltration (0 to 3 score range) from control and *Opa1*<sup>ΔIEC</sup> mice (*n* = 3 to 5 per group, means ± SD). Scale bars, 100 μm. (E) Representative colon sections from control and *Opa1*<sup>ΔIEC</sup> mice immunostained for MPO, F4/80, and CD4 (left; each shown in red, *n* = 5). Nuclei were counterstained with Hoechst 33342 (blue). Scale bars, 128 μm. Quantification of the staining was performed using Fiji/ImageJ (right). (F) mRNA expression relative to *Hprt* in colonic tissues from control and *Opa1*<sup>ΔIEC</sup> mice (*n* = 5, means ± SD). \**P* < 0.05; \*\**P* < 0.01; \*\*\**P* < 0.001; Mann-Whitney test [(C), (E), and (F)], unpaired Student's *t* test with Welch's correction (D), or two-way ANOVA with Tukey's correction (B) for comparison of the body weight.

significant changes between the stool microbiomes of *Opal<sup>fl/fl</sup>* and *Opal<sup>iΔIEC</sup>* mice before tamoxifen-mediated *Opal* deletion. In contrast, (tamoxifen-induced) *Opal*-deficient mice, when compared with control mice treated with tamoxifen, displayed marked microbial shifts as evidenced by alpha and beta diversity analysis and the analysis of differentially abundant taxa (fig. S5, A to D). Several of the differentially abundant amplicon sequence variants (ASVs) represented bacterial species with the potential to produce butyrate, a metabolite known to enhance intestinal barrier function (24). Among the five identified ASVs representing butyrate-producing bacteria, two were enriched and three were reduced in *Opal<sup>iΔIEC</sup>* mice (fig. S5E). Moreover, several of the taxa identified to be more abundant in *Opal<sup>iΔIEC</sup>* mice belong to Proteobacteria, a phylum comprising several species associated to IBD in humans.

### Epithelial OPA1 is a driver of gut barrier function and restricts microbiota-dependent gut inflammation

Further histological analysis of inflamed gut segments of *Opal<sup>iΔIEC</sup>* mice revealed intestinal crypts with extensive loss of epithelial cells, cryptitis, and crypt abscesses (Fig. 3A). Such extensive disruption of the crypt epithelial cell layer could compromise the integrity of the intestinal barrier and might allow microbial translocation from the gut lumen into the lamina propria (1). Fluorescence in situ hybridization (FISH) on intestinal samples from *Opal<sup>iΔIEC</sup>* mice, using a ribosomal RNA probe capable of labeling all eubacteria (EUB338), revealed the presence of bacteria within the epithelial cell layer and in the lamina propriae of *Opal<sup>iΔIEC</sup>* mice, whereas bacteria were only detected in the gut lumen in control mice (Fig. 3B). Furthermore, oral administration of 4-kDa fluorescein isothiocyanate (FITC)-dextran and subsequent measurement of serum fluorescence revealed increased intestinal permeability in *Opal<sup>iΔIEC</sup>* mice as compared with *Opal<sup>fl/fl</sup>* controls (Fig. 3C). This appeared to be an epithelial intrinsic effect, given that increased permeability was also observed in an IEC organoid model system (Fig. 3D).

Our data indicate that epithelial *Opal* deficiency leads to excessive microbial translocation from the gut lumen, thereby driving mucosal immune cell activation and inflammation. To directly test whether the spontaneous intestinal inflammation in *Opal<sup>iΔIEC</sup>* mice depended on the presence of intestinal microbiota, we depleted the microbiota in *Opal<sup>iΔIEC</sup>* and *Opal<sup>fl/fl</sup>* control mice using a well-established combination of four antibiotics. In the absence of antibiotic treatment, *Opal<sup>iΔIEC</sup>* mice lost weight (Fig. 3E) and developed signs of severe colitis as demonstrated by endoscopic and histologic analysis (Fig. 3F); antibiotic treatment largely prevented gut inflammation. This was further confirmed when comparing the colon length (Fig. 3G) and the expression of pro-inflammatory markers (Fig. 3H) in gut tissues. Antibiotic treatment did not affect any of these parameters and had no overt unwanted effects in control mice (Fig. 3, E to H) or in epithelial organoid cultures (fig. S6, A and B). Overall, microbiota depletion rescued *Opal<sup>iΔIEC</sup>* mice from spontaneously developing chronic intestinal inflammation, providing functional evidence for a microbiota-dependent pathology.

### OPA1 is required for epithelial cell differentiation and intestinal stem cell homeostasis

Our finding of epithelial barrier disruption after *Opal* ablation suggested an alteration in the cellular homeostasis of IECs. In support of this, terminal deoxynucleotidyl transferase-mediated deoxyuridine triphosphate nick end labeling (TUNEL) and cleaved caspase-3

staining revealed increased cell death in the colons of *Opal<sup>iΔIEC</sup>* mice compared with controls (Fig. 4A). Furthermore, the development of epithelial organoids from *Opal*-deficient gut tissues was impaired when compared with organoids generated from gut tissues of control mice (Fig. 4B). Likewise, cell death and caspase-3 activation were increased in *Opal*-deficient organoids when compared with control organoids (Fig. 4, B and C). A careful analysis of our histological images and our cell death analyses revealed that, along the crypt-villous axis, the lower crypt—where stem cells, Paneth cells, and cycling cells reside—was affected most. In support of this observation, *Opal<sup>iΔIEC</sup>* mice showed diminished expression of the stem cell markers *Lgr5* (*Gpr49*) and OLFM4 as well as significantly reduced proliferation in the lower crypt compartment, evidenced by 5-bromo-2'-deoxyuridine (BrdU) staining ( $P = 0.0047$ ) (Fig. 4, D and E). Similarly, in epithelial organoids derived from *Opal<sup>iΔIEC</sup>* mice, *Gpr49* and *Olfm4* along with the proliferation marker *Birc5* were reduced when compared with controls (Fig. 4F). Diminished expression of stem cell and proliferation markers was further demonstrated in epithelial organoids derived from *Opal<sup>iΔIEC</sup>* mice using immunohistochemical detection of KI67, 5-ethynyl-2'-deoxyuridine (EdU), and OLFM4 (fig. S7, A to C). The expression of markers of differentiated IECs, such as *Muc2* and ULEX for goblet cells and *Lyz1* and *Ang4* for Paneth cells, were increased in *Opal*-deficient organoids (Fig. 4F and fig. S7D). To systematically study epithelial changes induced by *Opal* deficiency, we next performed a bulk transcriptomic analysis of epithelial organoids generated from gut samples of *Opal<sup>iΔIEC</sup>* and control mice. In support of our qPCR and immunostaining results, we found an increase in genes attributed to secretory epithelial cell types, including Paneth cells, goblet cells, and enteroendocrine cells (Fig. 4G). In contrast, markers of transit-amplifying cells and stem cells were decreased in *Opal<sup>iΔIEC</sup>* when compared with control mice. Together, our data indicate a relative excess of differentiated epithelial cells at the expense of stem and progenitor cells.

### Opal-deficient epithelium lacks mitochondrial fusion and exhibits fragmented mitochondrial networks

To gain further insight into potential intrinsic changes at the gut barrier and in IECs induced by *Opal* deficiency, we next performed a bulk transcriptomic analysis of whole colon samples from *Opal<sup>iΔIEC</sup>* and control mice and performed a comparative gene ontology analysis of transcriptomic changes in whole colonic tissues and in pure epithelial cells, which was represented by our organoid RNA-seq dataset. Consistent with the spontaneous colitis in *Opal<sup>iΔIEC</sup>* mice, we observed transcriptomic changes in colonic tissues, with enrichment of genes related to inflammation and decreased expression of genes related to mitochondrial functions (Fig. 5A and fig. S8A) when compared with controls. In epithelial organoids, *Opal* deficiency was associated with increased expression of antimicrobial genes and decreased expression of genes related to mitochondrial functions (Fig. 5A and fig. S8A). *Opal* deficiency was associated with a specific down-regulation of mitochondrially expressed genes (Fig. 5B and fig. S8B) and that of genes related to metabolism and mitochondrial biogenesis (fig. S9, A and B). Because *Opal* deficiency has been reported to affect mtDNA copy number and mtDNA deletions (25), we next analyzed the mtDNA content in IECs of *Opal*-proficient and *Opal*-deficient organoids. Colonic tissue lysates from *Opal<sup>iΔIEC</sup>* mice showed an ~50% reduction in mtDNA content relative to nuclear DNA (Fig. 5C

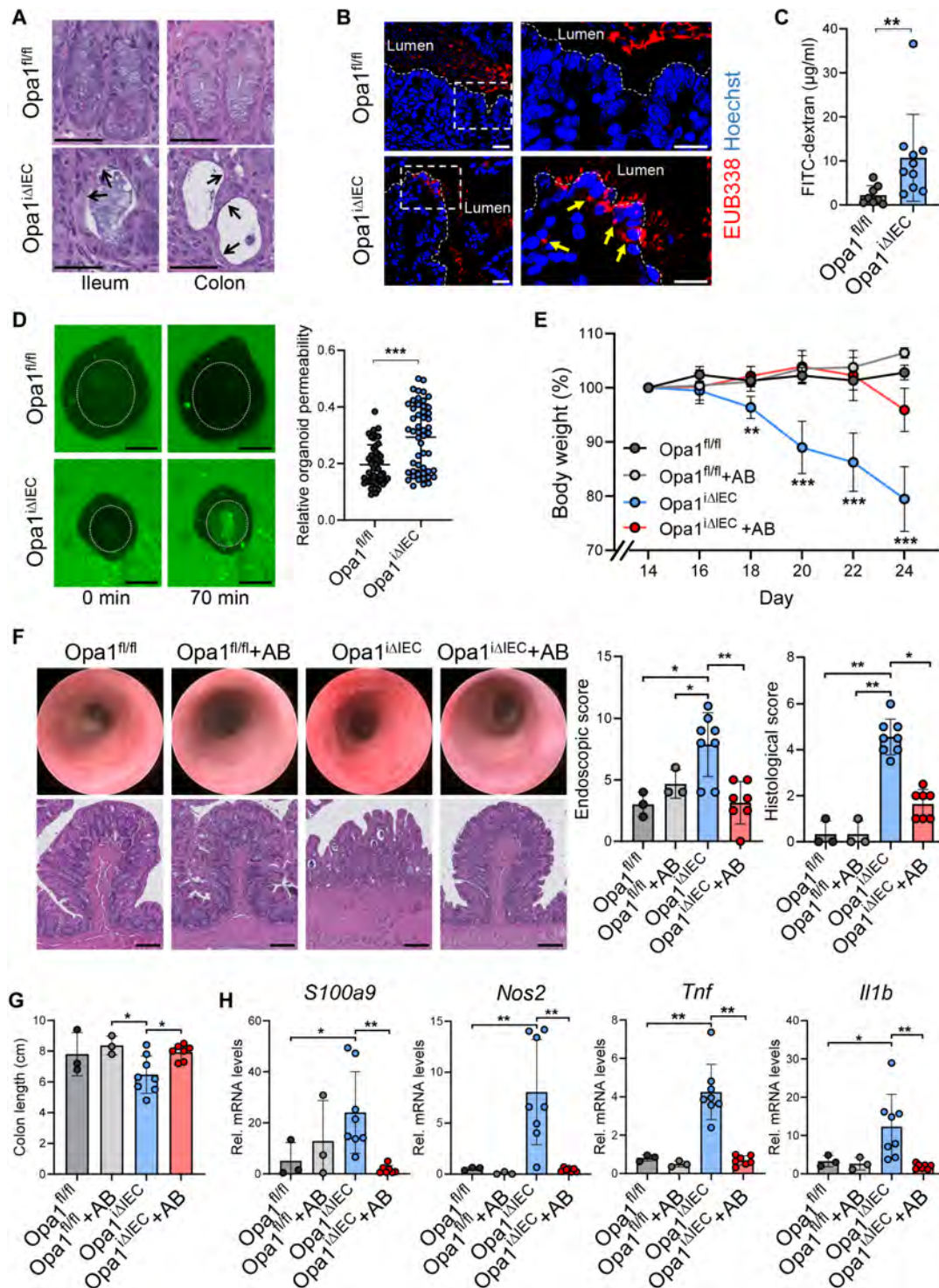


**Fig. 3. Chronic colitis in *Opa1<sup>ΔIEC</sup>* mice is microbiota dependent and associated with barrier dysfunction and microbial translocation.** (A) Representative H&E staining of the ileum and colon from control and *Opa1<sup>ΔIEC</sup>* mice (*n* = 7). Scale bars, 30 μm. Arrows indicate epithelial loss. (B) FISH to detect bacteria using the EUB338 probe (red) and colonic samples from control and *Opa1<sup>ΔIEC</sup>* mice. Nuclei were counterstained with Hoechst 33342 (blue). White dashed lines indicate the epithelial lining. Arrows indicate translocated bacteria (*n* = 5 to 7 per group). Scale bars, 25 μm. (C) Serum FITC-dextran amounts 4 hours after oral administration in control and *Opa1<sup>ΔIEC</sup>* mice (*n* = 8 to 10 per group, means ± SD). (D) Representative images of small intestinal organoids cultured in the presence of Lucifer yellow (green) as indicated (*n* = 3 independent experiments, means ± SD). Scale bars, 126 μm. White dashed circles indicate the lumen of the organoids. (E) Relative body weight (% of initial weight) of tamoxifen-induced *Opa1<sup>fl/fl</sup>* and *Opa1<sup>ΔIEC</sup>* mice with and without antibiotic (AB) treatment (*n* = 3 to 8 per group, means ± SD). (F) Representative endoscopic and histologic images (left) and scores (right) of mice with and without AB treatment (*n* = 3 to 8 per group, means ± SD). Scale bars, 100 μm. (G) Colon lengths are shown (*n* = 3 to 8 per group, means ± SD). (H) mRNA expression (relative to *Hprt*) in colonic samples from *Opa1<sup>fl/fl</sup>* and *Opa1<sup>ΔIEC</sup>* mice with or without AB treatment (*n* = 3 to 8 per group, means ± SD). \**P* < 0.05; \*\**P* < 0.01; \*\*\**P* < 0.001; Mann-Whitney test [(C) and (D)] or two-way ANOVA with Tukey's correction [(E), (F), (G), and (H)] for multiple comparisons.

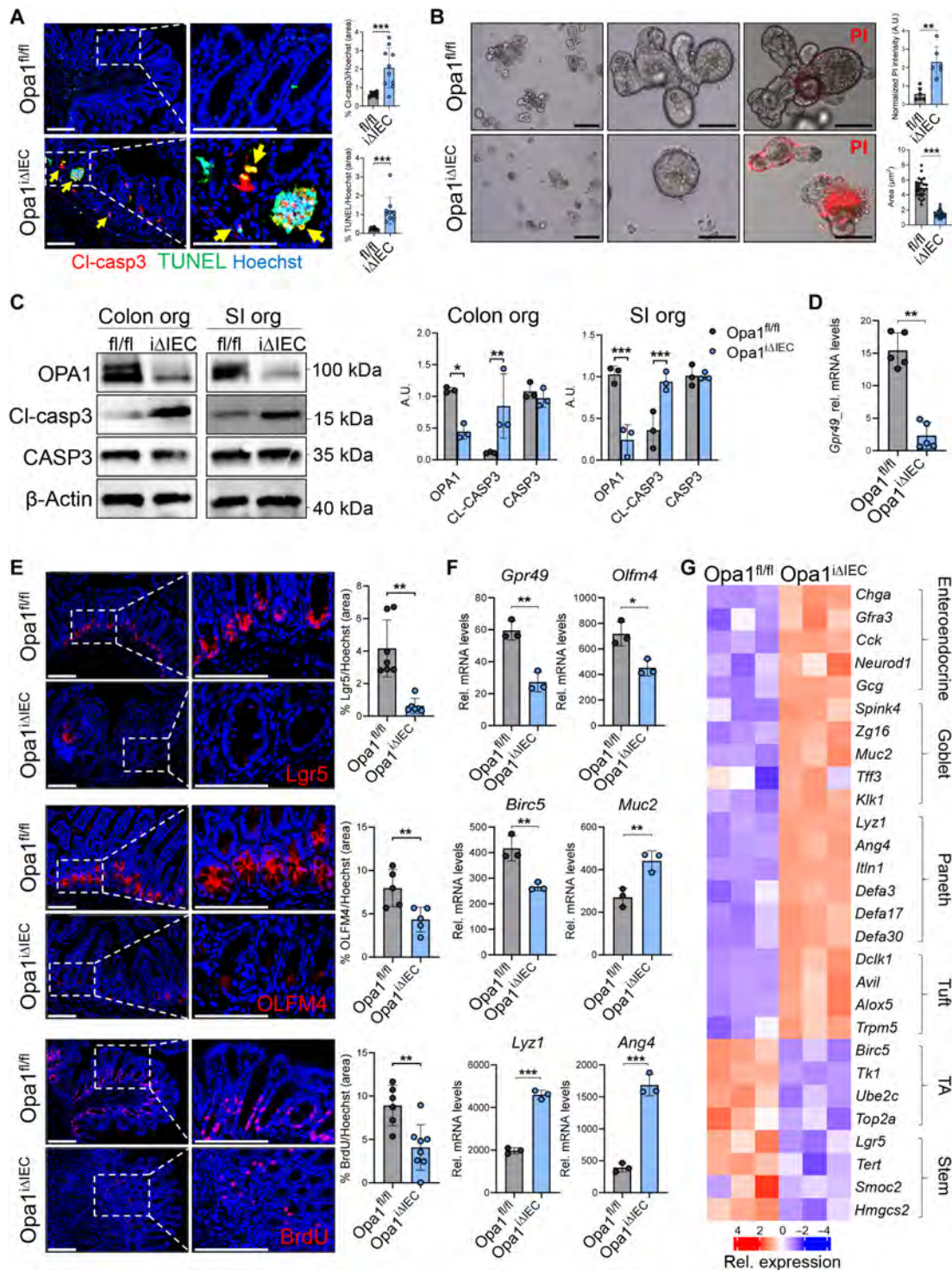


**Fig. 4. OPA1 is required for epithelial cell differentiation and intestinal stem cell homeostasis.** (A) Representative immunofluorescence images (left) and quantification (right) of cleaved caspase-3 (Cl-casp3; red) and TUNEL (green) detection in control and *Opa1*<sup>ΔIEC</sup> colon sections (*n* = 10). Nuclei were stained with Hoechst 33342 (blue). Scale bars, 128 μm. Arrows indicate double-positive cells. (B) Representative images of small intestinal organoids from *Opa1*<sup>fl/fl</sup> and *Opa1*<sup>ΔIEC</sup> mice treated with 4-OHT in vitro (scale bars, 250 μm) and stained with PI (red) (left). PI intensity and the surface area were quantified (right) in 4-OHT-treated (3 days) small intestinal (SI) and colon organoids (*n* = 3) with independent experiments. (C) Protein expression (left) and quantification (right) in 4-OHT-treated (3 days) small intestinal (SI) and colon organoids (*n* = 3) with independent experiments. β-Actin was used as a loading control. (D) Relative *Gpr49* mRNA expression in the colons of control and *Opa1*<sup>ΔIEC</sup> mice (*n* = 5, means ± SD). (E) Representative images (left) and quantification (right) of *Lgr5*, OLFM4, and BrdU (each red) on small intestinal (OLF4) and colon (*Lgr5* and BrdU) sections. Immunohistochemistry was used to detect OLFM4 and BrdU. *Lgr5* mRNA was detected by RNAscope. Sections were counterstained with Hoechst 33342 (blue) (*n* = 5 to 8 per group). (F) qPCR analysis using mRNA from control and *Opa1*<sup>ΔIEC</sup> small intestinal organoids (*n* = 3) independent experiments, means ± SD). (G) Heatmap showing the expression of IEC marker genes in small intestinal organoids from *Opa1*<sup>fl/fl</sup> and *Opa1*<sup>ΔIEC</sup> mice (*n* = 3). Colors (red, up; blue, down) depict relative expression. \**P* < 0.05; \*\**P* < 0.01; \*\*\**P* < 0.001; Mann-Whitney test [(A), (B), (D), and (E)], unpaired Student's *t* test with Welch's correction (F), or two-way ANOVA with Sidák correction (C).



and table S3), providing further evidence for a disruption of mitochondrial homeostasis. TEM revealed alterations in the *Opal*-deficient intestinal epithelium, showing small circular mitochondria and decreased cristae density, whereas in control animals, the mitochondria were smooth, more electron-dense with extensive cristae networks, and had a less circular appearance (Fig. 5D). The observed changes in mitochondrial shape and structure in *Opal*<sup>iΔIEC</sup> epithelial cells were similar to those observed in epithelial cells of samples from patients with IBD (Fig. 1A and fig. S1, A and B). Moreover, in IECs of control mice, but much less in *Opal*<sup>iΔIEC</sup> mice, we frequently observed elongated mitochondria, branched mitochondria, and neighboring mitochondria with electron-dense contact sites (Fig. 5D and fig. S9C), indicating different stages of mitochondrial fusion, according to the criteria described by Bereiter-Hahn and Voth (20). Moreover, 2D primary epithelial organoids grown from *Opal*<sup>iΔIEC</sup> mice and stained with MitoTracker Deep Red showed fragmentation of the mitochondrial network compared with organoids from control mice (Fig. 5E), a finding further underlining aberrant mitochondrial dynamics in *Opal*-deficient IECs. Mitochondrial fragmentation was also observed in MC38 colonic cells after CRISPR-Cas9-mediated deletion of *Opal* (fig. S10A). To elucidate mitochondrial structures at high optical resolution, we recorded images of gut samples using cytochrome c oxidase subunit 4 (COX4) as a mitochondrial marker (Fig. 5, F and G, and fig. S10B), followed by a computer-aided analysis of mitochondrial density and size. Super-resolution spinning disk microscopy confirmed structural difference with reduced tubeness and increased fragmentation of mitochondria in gut samples of *Opal*<sup>iΔIEC</sup> mice compared with controls (Fig. 5G and movie S1). Functional studies using epithelial organoids grown from human gut biopsies and treated with the OPA1 inhibitor MYLS22 demonstrated mitochondrial fragmentation (Fig. 5H), diminished mitochondrial gene expression (fig. S10C and table S4), and decreased expression of epithelial progenitor markers *GPR49* (LGR5) and *KI67* (Fig. 5I), thus mimicking our findings in *Opal*<sup>iΔIEC</sup> mice.

Mitochondrial fragmentation is associated with impaired mitochondrial function and increased cellular and metabolic stress (26, 27). In line with this, we observed increased reactive oxygen species (ROS) production in epithelial organoids derived from *Opal*<sup>iΔIEC</sup> mice when compared with controls (Fig. 6A). To evaluate key parameters of mitochondrial function in *Opal*-deficient IECs, we performed Seahorse analysis of two-dimensional (2D)-grown organoids from *Opal*<sup>iΔIEC</sup> and control mice. Our analyses indicated that *Opal* deficiency caused a significant decline in the oxygen consumption rate (OCR), indicated by the decreased ATP-linked respiration ( $P = 0.0159$ ), basal respiration ( $P = 0.0079$ ), and maximal respiration ( $P = 0.0079$ ), as well as by reduced proton leak ( $P = 0.0159$ ), demonstrating that *Opal* deletion causes depletion of the cellular capability for energy supply in IECs (Fig. 6B). Our data further show that the fraction of ATP production derived from mitochondria within the total cellular ATP production was significantly decreased ( $P = 0.0092$ ) in *Opal*-deficient IECs compared with controls (Fig. 6C) and was associated with diminished mitochondrial membrane potential in both 2D-grown epithelial organoids from *Opal*<sup>iΔIEC</sup> mice (Fig. 6D) and in an *Opal*-deficient cell line (fig. S10D).

Mitochondrial fragmentation is dependent on the dynamin-related protein 1 (DRP1), which is essential for the segregation of damaged mitochondria and their targeting to mitophagy (13, 16).

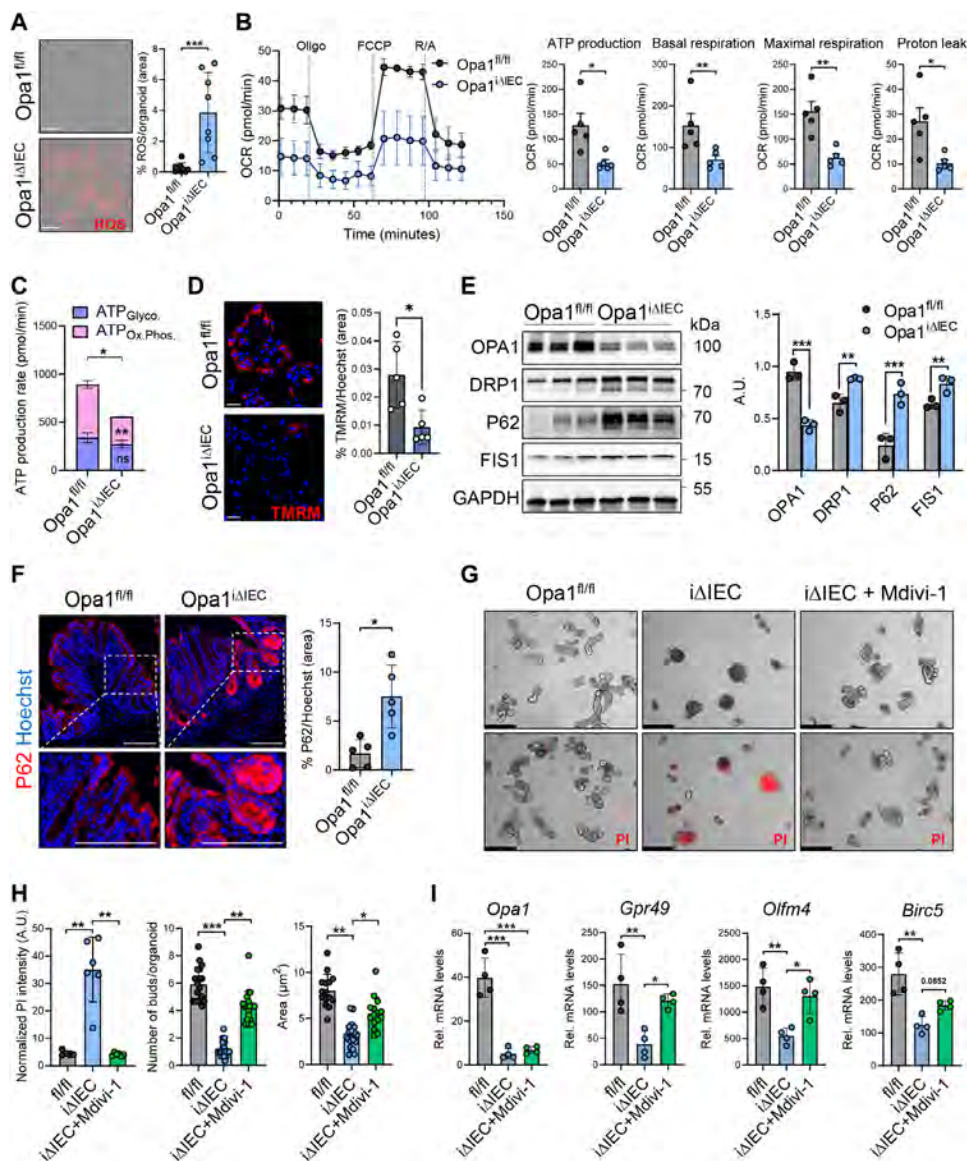
We observed increased expression of DRP1 and the fission mediator FIS1 along with an increase in the mitophagy marker P62 in the colonic tissues of *Opal*<sup>iΔIEC</sup> mice and in epithelial organoids (Fig. 6, E and F, and fig. S10E). P62 staining was particularly abundant in the lower crypt (Fig. 6F). When using the fission inhibitor Mdivi-1, which targets DRP1, we could partially rescue the diminished organoid development and the increased IEC death observed in the absence of *Opal* (Fig. 6, G and H). Moreover, Mdivi-1 treatment restored the expression of stem and progenitor cell markers in *Opal*-deficient organoids (Fig. 6I). Similar results were obtained with organoids treated with or without P110, another inhibitor of DRP1-mediated mitochondrial fission (fig. S11, A and B). Thus, our experimental data are consistent with a model in which deficient mitochondrial fusion in IECs leads to DRP1-dependent fragmentation of the mitochondrial network, increased epithelial cell death with barrier dysfunction, microbial translocation, and consequential chronic intestinal inflammation.

## DISCUSSION

Our study demonstrates that mitochondrial aberrations, such as previously reported in samples from patients with IBD, can originate from impaired *Opal*-dependent mitochondrial fusion in the gut epithelium. We further provide evidence that the lack of the mitochondrial fusion molecule OPA1 in the gut epithelium leads to impaired epithelial barrier function and translocation of bacteria into the lamina propria. Our study also demonstrated that this is critical for gut immune homeostasis because deficiency for *Opal* in mice leads to the spontaneous development of inflammation in the ileum and colon, the gut segments most frequently affected in patients with IBD.

Several lines of evidence support an important role for mitochondria in the pathogenesis of IBD. Approximately 5% of IBD susceptibility genes identified in genome-wide association studies have a direct role in regulating mitochondrial functions (7). Studies in pediatric patients with UC showed a marked suppression of mitochondrial genes (21). Enterocytes of patients with IBD have been described as exhibiting rounded mitochondria with irregular cristae (2–4, 28), indicative of the fragmentation of the cellular mitochondrial network in IECs. Our findings confirmed and detailed these reports, demonstrating fragmentation of the mitochondrial network in both CD and UC. Although mitochondrial dysfunction appears to be a feature of IBD, the mechanisms of mitochondrial dysregulation and fragmentation in IBD have largely remained unknown. Fragmentation of the mitochondrial network can have different causes, one being irregular mitochondrial fusion and fission. Our electron microscopy studies revealed roundish mitochondria in epithelial cells of patients with either UC or CD, whereas epithelial cells of uninflamed control individuals showed a dense network of elongated and branched mitochondria, ultrastructural features that have been associated with mitochondrial fusion (20). We found a high degree of similarity between the ultrastructural appearance of mitochondria in IECs from *Opal*<sup>iΔIEC</sup> mice and those in IBD samples. In further support of a role for dysregulated mitochondrial fission and fusion in the gut epithelia of patients with IBD, we observed changes in the gene expression pattern of key molecules driving these processes. Whereas these expression changes were more evident in UC samples than in CD samples, we observed changes in mitochondrial shape and mitochondrial gene expression in both

**Fig. 6. Impaired cellular homeostasis in *Opa1*-deficient IECs can be rescued by inhibition of DRP1.** (A) Representative images (left) and quantification (right) of control and *Opa1*<sup>ΔIEC</sup>-derived 2D-grown small intestinal organoids stained with the oxidative stress detection reagent to visualize ROS (red) (*n* = 3 independent experiments with 2 or 3 fields of view each, means ± SD). Scale bars, 36 μm. (B) Cellular OCRs and (C) ATP production rates are shown in control and *Opa1*<sup>ΔIEC</sup> small intestinal organoids (each *n* = 5 per group, means ± SD). (D) Representative images of tetramethylrhodamin methyl ester (TMRM; red)-stained *Opa1*<sup>fl/fl</sup> and *Opa1*<sup>ΔIEC</sup> 2D-grown small intestinal organoids to indicate mitochondrial membrane potential (*n* = 5, means ± SD). Nuclei were stained with Hoechst 33342 (blue). Scale bars, 50 μm. (E) Western blot using the colon tissue lysates of control and *Opa1*<sup>ΔIEC</sup> mice (left) and quantification (right). GAPDH (glyceraldehyde-3-phosphate dehydrogenase) was used as a loading control for normalization (*n* = 3, means ± SD). (F) Representative images (left) of P62 (red)-stained colon tissue sections from control and *Opa1*<sup>ΔIEC</sup> mice and quantification (right). Nuclei were stained with Hoechst 33342 (blue). Scale bars, 128 μm. (G) Representative PI staining (red) of intestinal organoids with or without Mdivi-1 treatment. Scale bars, 250 μm. (H) Quantification of organoid area, number of buds per organoid, and PI staining intensity (*n* = 5 independent experiments; means ± SD). (I) mRNA expression relative to *Hprt* in intestinal organoids of *Opa1*<sup>fl/fl</sup> and *Opa1*<sup>ΔIEC</sup> mice with or without Mdivi-1 treatment (*n* = 4; means ± SD). \**P* < 0.05; \*\**P* < 0.01; \*\*\**P* < 0.001; Mann-Whitney test [(A), (B), (C), (D), and (F)], unpaired Student's *t* test with Welch's correction (E), or two-way ANOVA with Tukey's correction [(H) and (I)] for multiple comparison.



UC and CD, indicating that mitochondrial dynamics might be regulated through various mechanisms.

The expression of *OPA1* is tightly controlled through both transcriptional and posttranscriptional mechanisms to ensure proper mitochondrial dynamics. Transcriptionally, *OPA1* expression is regulated by metabolic cues and oxidative stress (29, 30). Posttranscriptionally, *OPA1* is subject to alternative splicing, producing several isoforms with distinct roles in mitochondrial fusion (31, 32). In addition, proteolytic processing of *OPA1* by mitochondrial proteases, such as *OMA1* and *YME1L*, modulates its activity and affects mitochondrial fission and fusion (33–35). This complex regulation ensures that *OPA1* can rapidly respond to cellular demands, maintaining mitochondrial integrity and function under varying physiological conditions.

In our study, mitochondrial structural changes were observed particularly in areas of active inflammation, a finding that aligns well with a recent report by Alula *et al.*, who described mitochondrial aberrations in Paneth cells, goblet cells, and enterocytes in the

inflamed ilea of patients with CD (28). The reduced expression of *OPA1*, *MFN1*, and *MFN2* and that of mitochondrial genes correlated negatively with the degree of inflammation in patients with UC in our own cohort. Moreover, reduced expression of mitochondrial fusion genes was observed in publicly available single-cell transcriptomic data from inflamed UC patient samples not only when compared with healthy individuals but also when compared with uninflamed samples from patients with IBD. Together, this suggests that dysregulated mitochondrial dynamics is a feature of inflammation in IBD that perpetuates this chronic disease rather than being a causative factor. Our data are consistent with a model in which dysregulated fusion drives a vicious cycle that compromises epithelial barrier function, promoting further inflammation and dysregulation of mitochondrial dynamics.

Our data suggest that increased mitochondrial fission and fragmentation contribute to the impact of *Opa1* deletion in IECs. First, we observed an increased expression of *FIS1* protein and mitochondrial fragmentation in *Opa1*-deficient organoids. Second,

pharmacological inhibition of DRP1/FIS1 rescued the homeostatic defects in *Opal*-deficient organoids. Consistent with our conclusions, the administration of P110, a DRP1 GTPase inhibitor, was recently reported to have protective effects in a short-term model of chemically induced colitis (36).

Our study underlines that the gut epithelium, which acts as a barrier between the luminal environment and the underlying tissues, relies heavily on mitochondrial function for its integrity and proper functioning. The gut epithelium is particularly vulnerable to oxidative stress, and dysfunctional mitochondria can be a major source of ROS (8, 37, 38). In line with these studies, we observed increased ROS production in IECs of *Opal*<sup>iΔIEC</sup> mice.

mtDNA, unlike nuclear DNA, is particularly susceptible to stress-induced damage (39, 40), and failure to efficiently repair mtDNA damage can escalate the production of ROS and trigger mitochondrial dysfunction. The process of mitochondrial fusion has been reported to play a pivotal role in compensating for defects in mitochondria containing damaged mtDNA (41–43). Through mitochondrial fusion, critical functional and structural components, such as mtDNA, proteins, and lipids, can be exchanged and shared between mitochondria to ameliorate the effects of environmental or inflammatory stress on mitochondrial function (44). Mitochondrial shape changes, such as those described here, are closely linked to metabolic stress, where shifts in metabolism can both trigger and be a consequence of changes in mitochondrial morphology (27). Metabolically stressed epithelia have been described to show compromised barrier integrity (45). In a model of chemically induced acute colitis, mice deficient for PGC1 $\alpha$ , a key regulator of mitochondrial biogenesis and energy metabolism, developed more severe colitis as compared with controls (46). However, PGC1 $\alpha$ -deficient mice were phenotypically normal and did not develop spontaneous inflammation. Although compensatory mechanisms might limit the phenotypic effect in PGC1 $\alpha$ -deficient mice, one might conclude that changes in mitochondrial mass alone cannot explain the severe spontaneous inflammation in *Opal*<sup>iΔIEC</sup> mice.

Our data further demonstrate that the severe spontaneous inflammation observed in *Opal*<sup>iΔIEC</sup> mice depended on the presence of microbiota, ruling out that mitochondrial stress driven by impaired mitochondrial fusion in IECs alone would be sufficient to cause inflammation in this model. Of note, the gut inflammation developing in *Opal*<sup>iΔIEC</sup> mice was largely restricted to the colon and ileum, the two gut parts most frequently affected in patients with IBD and those with the highest load of microbes present. Changes in the gut microbiota have been demonstrated in patients with IBD. For example, a reduced abundance of butyrate-producing bacteria has recently been associated with CD (47). In our studies, deletion of *Opal* was associated with shifts in microbial composition, including increased amounts of Proteobacteria and alterations in the number of butyrate-producing bacteria. Although it is likely that this shift is a consequence of disrupted epithelial homeostasis and function, our studies do not exclude that the altered microbiome in *Opal*<sup>iΔIEC</sup> mice contributes to the persistent spontaneous inflammation observed in these animals.

Our studies further demonstrated depletion of epithelial progenitor cells, such as stem cells and transit-amplifying cells, along with increased cell death and mitophagy specifically in the lower crypt area, where stem cells and Paneth cells reside. It is likely that balanced mitochondrial dynamics is particularly important in epithelial stem cells and longer-lived Paneth cells. In line with these

conclusions, a previous study demonstrated that mice with an epithelium-specific deletion of prohibitin, a pleiotropic protein implicated in fundamental cellular processes, including mitochondrial function and proliferation, exhibited aberrant Paneth cells and spontaneous development of ileitis in mice (8). Mitochondrial stress, reduced stem cell numbers, and abnormal Paneth cells were also observed in mice with a stem cell-specific deletion of *Hsp60* (9), providing additional support for a key role of mitochondrial health in stem cells and Paneth cells of the lower crypt. Mitochondrial health might be particularly crucial in intestinal stem cells and Paneth cells because of their relatively long life span, which might allow an accumulation of damaged mitochondria in these cells (48). Thus, mitochondrial fission and fusion as repair processes might be particularly important in these cell types. In contrast, enterocytes and goblet cells have a much shorter life span of 3 to 5 days, which might naturally prevent the impact of an accumulation of damaged mitochondria in these cells.

Our study has several limitations: First, *OPA1* has so far not been identified as an IBD risk gene in genome-wide association studies. Second, other mitochondrial dynamics-related proteins and pathways that may contribute to IBD pathogenesis remain unexplored. Third, whereas *OPA1* is a key molecule for mitochondrial fusion, it has also been reported to regulate the structure of the inner mitochondrial membrane and the formation of cristae (32). Last, the pharmacological intervention targeting DRP1 showed partial effects. Thus, it cannot be ruled out that additional compensatory mechanisms may influence mitochondrial dynamics and barrier function. Further investigation, particularly in human cohorts and with more refined therapeutic models, is needed to confirm and extend these findings.

Collectively, our study confirms previous reports of mitochondrial dysfunction in IBD and provides evidence that dysregulated fission and fusion in the gut epithelium might be causative of mitochondriopathy in these patients. Our study highlights a role for epithelial *OPA1* and mitochondrial fusion in maintaining an efficient intestinal barrier and in preventing excessive microbial confrontation of the mucosal immune system by bacterial antigens in vivo. A deeper understanding of these processes might pave the way to better therapeutic approaches for individuals with IBD.

## MATERIALS AND METHODS

### Study design

The objective of this study was to evaluate the impact of mitochondrial dynamics in IBD. On the basis of initial findings in patients with IBD and mice with experimental colitis that showed dysregulated expression of genes associated with mitochondrial fusion, we hypothesized that changes in mitochondrial dynamics might underlie the mitochondriopathy previously reported in IBD. We evaluated this hypothesis analyzing gene expression in our own cohort of patients with either UC or CD and in publicly available transcriptome data of patients with IBD, electron microscopy of control and patient samples, and studies using gut organoids grown from patient samples. We furthermore performed controlled laboratory experiments in *Opal*<sup>iΔIEC</sup> mice lacking the fusion regulator *Opal* specifically in IECs and respective *Opal*<sup>fl/fl</sup> controls and in C57BL/6 mice induced to develop experimental intestinal inflammation by either DSS, oxazolone, or adoptive T cell transfer. In vivo experiments, *Opal*<sup>iΔIEC</sup> mice and *Opal*<sup>fl/fl</sup> controls were treated

with antibiotics to deplete the gut microbiota. Gut samples from *Opa1<sup>ΔIEC</sup>* and control mice were analyzed using weight monitoring, endoscopy, histology, IHC, bulk transcriptomics, qPCR, and Western blotting. Cells and intestinal organoids grown from these mice were studied in vitro using inhibitors of mitochondrial fission (Mdivi-1 and P110) in organoid experiments. Last, cell lines lacking *OPA1* were generated and compared with controls. The sample sizes were established on the basis of previously published works from our laboratory and comparable studies in the field. All instances of replication described in this study refer to biological replicates (individual human samples or mice). Animals were either littermates in the same cage (*Opa1<sup>ΔIEC</sup>* and control mice) or were randomly allocated to either an experimental or control group. Data collection was conducted in a blinded manner. Animal studies were approved by the Ethics Committee of the Friedrich-Alexander-Universität Erlangen-Nürnberg and the Ethics Commission of Lower Franconia. Mouse experiments were terminated for animals that met any of the following intermediate end points: (i) weight loss of 20% or more, (ii) bloody diarrhea, and (iii) abdominal cramping. Mice reaching these end points were immediately euthanized. One outlier was identified in Fig. 1F using a Grubbs' test in GraphPad Prism and excluded from the study during the reviewing process.

### Animals

Mice carrying loxP-flanked *Opa1* alleles (*Opa1<sup>fl/fl</sup>*) (18) were crossed with *Villin-CreERT2* mice to generate inducible mice lacking *Opa1* specifically in IECs (*Opa1<sup>ΔIEC</sup>*). Mice negative for the expression of *Villin-CreERT2* served as controls in all experiments and are designated *Opa1<sup>fl/fl</sup>*. To induce *Opa1* deletion in the intestinal epithelium, tamoxifen (Sigma-Aldrich; 75 mg/kg of mouse body weight) was injected for five consecutive days. In all experiments, *Opa1<sup>fl/fl</sup>* littermates injected with tamoxifen served as controls. All experiments were performed with age-matched mice (8 and 12 weeks of age) of both sexes. Where applicable, mice were randomized into groups. Mice were maintained under light- and temperature-controlled conditions and monitored by analysis of weight loss, endoscopic score, diarrhea score, and rectal bleeding. Isoflurane (1.5%) in oxygen was used during endoscopy.

For antibiotic administration, *Opa1<sup>ΔIEC</sup>* mice received autoclaved water containing ampicillin (1 g/liter; Ratiopharm), neomycin (1 g/liter; Caesar & Loretz GmbH), metronidazole (1 g/liter; Braun), and vancomycin (0.5 g/liter; Eberth Arzneimittel GmbH) 4 days before tamoxifen application until the end of the experiment. Control mice received autoclaved water without antibiotics. Serial dilutions of dissolved stool pellets were plated on LB agar plates. After 24 hours of incubation at 37°C, bacterial colonies were evaluated to confirm microbiota depletion.

Mini-colonoscopy was performed, and colonic inflammation was analyzed and categorized as previously described using the murine endoscopic index of colitis severity (MEICS) score (49). In brief, mice were anesthetized with 1.5% isoflurane, and changes in colon wall thickening, vascular pattern, the presence of fibrin, mucosal granularity, and stool consistency were assessed using the COLOVIEW System (Karl Storz).

For in vivo imaging (IVIS), mice were anesthetized with 1.5% isoflurane, and L-012 (25 mg/kg mouse body weight; Wako Chemicals) was administered by intraperitoneal injection. After 15 min, luminescence was measured using an in vivo imaging IVIS Spectrum CT

system (PerkinElmer). Quantification was performed using the software Living Image 4.0.

### Induction of experimental colitis in mice

Experimental colitis in mice was induced following previously described protocols (50, 51). C57BL/6J mice (Janvier) were used as wild-type mice in the following experimental models. In brief, for acute DSS-induced colitis, mice were administered 3% DSS (MP Biomedicals) in their drinking water for 6 to 8 days. Mice were then either euthanized or subjected to normal water to allow recovery. To induce chronic colitis, we subjected mice to three cycles of 2% DSS (MP Biomedicals), each lasting 5 to 7 days, followed by a 2-week recovery phase in which the mice received regular water. To induce the adoptive transfer colitis model, we isolated CD4<sup>+</sup> CD25<sup>-</sup> T cells from the spleens of wild-type mice using magnetic cell sorting-based isolation (CD4<sup>+</sup> T Cell Isolation Kit, mouse, Miltenyi Biotec) with additional CD25-negative selection (CD25 MicroBead Kit, mouse, Miltenyi Biotec). The viability and purity of the isolated cells were confirmed by flow cytometry, and 1 million cells were then injected intraperitoneally into Rag1<sup>-/-</sup> mice on a C57BL/6J background. Mice were euthanized 3 weeks after T cell transfer. The induction of inflammation in the oxazolone colitis model requires a preliminary sensitization step, where a 3% (w/v) solution of 4-ethoxymethylene-2-phenyl-2-oxazolone-5-one (oxazolone; Sigma-Aldrich) in a 1:4 dilution with an olive oil/acetone mixture was applied to the shaved skin of the mice. Seven days after the sensitization procedure, a 150- $\mu$ l intrarectal enema of 0.5% oxazolone in 50% ethanol was administered. Mice were euthanized 24 hours later. Evaluation of colitis development involved measuring body weight loss and clinically assessing inflammation symptoms. Endoscopic analysis was performed to systematically evaluate colitis parameters as described before. Tissue samples from the distal colon were collected upon necropsy for further analyses.

### Human samples

Fresh endoscopic colon biopsies of control individuals and patients with IBD were obtained from the Universitätsklinikum Erlangen for TEM and isolation of human organoids. Paraffin-embedded samples from the colons of control individuals and patients with IBD were obtained from the Gastroenterology Department of the Charité Universitätsmedizin Berlin (table S1). An overview of patient characteristics of the IBDome cohort (v0.50) used for transcriptomics is provided in table S2. All human material used in this study was obtained after informed written consent of the donors and after approval by the Ethics Committees of the Friedrich-Alexander-Universität Erlangen-Nürnberg and the Charité Universitätsmedizin Berlin in accordance with all relevant ethical regulations. Written informed consent was obtained from the patients, and all data were anonymized.

### Isolation and culture of 3D and 2D intestinal organoids

Intestinal crypts were freshly isolated from full-length mouse small intestine or colon or from human colonic biopsies and cultured for a total of 6 days in Matrigel (BD Bioscience) in 48-well plates with 350  $\mu$ l of a medium as previously described (52). Briefly, the mouse intestine was cut into small pieces and incubated in 2 mM EDTA for 30 min to release the crypts. Crypts were filtered through a 70- $\mu$ m strainer and embedded in Matrigel with a culture medium containing 10% R-spondin1 conditioned medium, 5% Noggin conditioned

medium, B27 (Gibco), *N*-acetylcysteine (1 mM; Sigma-Aldrich), primocin (50 µg/ml; InvivoGen), and epidermal growth factor (50 ng/ml; ImmunoTools). For culturing the human intestinal organoids, WNT-3A (0.25 nM; PeproTech), IGF-1 (100 ng/ml; PeproTech), SB202190 (10 µM; MedChemExpress), Y-27632 (10 µM; Selleckchem), A8301 (500 nM; Hycultec), and nicotinamide (10 mM; Sigma-Aldrich) were supplemented on top of the mouse organoid culture medium. In some experiments, organoids were treated with 4-hydroxytamoxifen (4-OHT; 200 nM; Selleckchem) for at least 3 days to induce *Opa1* deletion (*Opa1*<sup>iAIEC</sup>). Human colon organoids were treated with the *Opa1* inhibitor MYLS22 (50 µM; MedChemExpress) for 24 hours. In some experiments, mouse intestinal organoids were stimulated for 24 hours with the Drp1 inhibitor Mdivi-1 (10 µM; Bio-Techne Tocris) or P110 (1 µM; Bio-Techne Tocris). To generate organoid-derived monolayers (2D-grown organoids), we disrupted fully grown organoids by pipetting with TrypLE Express1x (Gibco) and incubated at 37°C for 5 min. Crypt pellets were resuspended in human IntestiCult (STEMCELL) and seeded into Matrigel-coated 24-well plates or ibidi 8-well µ-slides (ibidi GmbH). Growth of organoids and intestinal epithelial monolayers was monitored using a light microscope.

### Organoid permeability assay

Small intestinal organoids were freshly isolated as described above and plated in ibidi 8-well µ-slides (ibidi GmbH). After 2 days of 4-OHT (200 nM; Selleckchem) treatment, Lucifer yellow (LY; 1 mM; Sigma-Aldrich) was added to the medium for live cell imaging with 5% CO<sub>2</sub> at 37°C using a Leica TCS-SPE live cell observer (Leica). EGTA (2 mM; Merck) was added to the medium after 70 min to ensure that the imaged organoids were able to take up the LY from the medium. Luminal fluorescence intensity was normalized to the mean total fluorescence intensity using the Fiji/ImageJ software as previously described (53).

### PI staining in organoids

Propidium iodide (PI; 5 µg/ml) was added to the organoid medium for 10 min. Images of organoid staining were captured by fluorescence microscopy using the DMI 4000 B microscope (Leica). Quantification of staining was performed using Fiji/ImageJ.

### FITC-dextran permeability experiments

Mice were fasted overnight (12 hours) and then administered FITC-dextran (4 kDa; Sigma-Aldrich) (4 mg/10 g of mouse body weight) for 4 hours. Mice were anesthetized, and blood was collected by cardiac puncture and centrifuged at 4000 rpm for 15 min to obtain a serum. The fluorescence intensity of each serum sample (100 µl) was measured using Infinite M200 (Tecan) with the excitation at 490 nm and emission at 520 nm.

### Generation of *OPA1* knockout cells

MC38 and HT29 cells were cultured in complete Dulbecco's modified Eagle's medium (Gibco) containing 10% fetal bovine serum, penicillin (100 U/ml), and streptomycin (100 µg/ml) at 37°C in a 5% CO<sub>2</sub> incubator. *OPA1* knockout (KO) cells were generated by CRISPR-Cas9 using either *Opa1* or *OPA1* CRISPR-Cas9 plasmids (Santa Cruz Biotechnology), respectively. After transfection, green fluorescent protein-positive cells were sorted by flow cytometry (FACSAria II; BD) and cultured as single-cell colonies in 96-well plates. KO of *OPA1* was validated by Western blot analysis.

### Statistical analysis

Data were analyzed using GraphPad Prism 10 (GraphPad software). As described in the corresponding figure legends, two-tailed Student's *t* test or nonparametric Mann-Whitney test was used to test for significance between two groups. For grouped data, Kruskal-Wallis test followed by Dunn's multiple comparisons or two-way analysis of variance (ANOVA) with Tukey's or Sidák correction was used. Significance is indicated as \**P* < 0.05, \*\**P* < 0.01, and \*\*\**P* < 0.001. All data are presented as means ± SD. The Fiji/ImageJ software was used to perform statistics for immunohistochemical staining, Western blots, mitochondrial length, and the organoid luminal fluorescence intensity.

### Supplementary Materials

#### The PDF file includes:

Materials and Methods

Figs. S1 to S11

Tables S1 to S4

References (54, 55)

#### Other Supplementary Material for this manuscript includes the following:

Movie S1

Data file S1

MDAR Reproducibility Checklist

### REFERENCES AND NOTES

1. J. V. Patankar, C. Becker, Cell death in the gut epithelium and implications for chronic inflammation. *Nat. Rev. Gastroenterol. Hepatol.* **17**, 543–556 (2020).
2. G. Delpre, I. Avidor, R. Steinhilber, U. Kadish, M. Ben-Bassat, Ultrastructural abnormalities in endoscopically and histologically normal and involved colon in ulcerative colitis. *Am. J. Gastroenterol.* **84**, 1038–1046 (1989).
3. A. Nazli, P.-C. Yang, J. Jury, K. Howe, J. L. Watson, J. D. Söderholm, P. M. Sherman, M. H. Perdue, D. M. McKay, Epithelia under metabolic stress perceive commensal bacteria as a threat. *Am. J. Pathol.* **164**, 947–957 (2004).
4. C. Günther, E. Martini, N. Wittkopf, K. Amann, B. Weigmann, H. Neumann, M. J. Waldner, S. M. Hedrick, S. Tenzer, M. F. Neurath, C. Becker, Caspase-8 regulates TNF- $\alpha$ -induced epithelial necroptosis and terminal ileitis. *Nature* **477**, 335–339 (2011).
5. E. A. Novak, K. P. Mollen, Mitochondrial dysfunction in inflammatory bowel disease. *Front. Cell Dev. Biol.* **3**, 62 (2015).
6. W. E. W. Roediger, The colonic epithelium in ulcerative colitis: An energy-deficiency disease? *Lancet* **316**, 712–715 (1980).
7. G.-T. Ho, R. E. Aird, B. Liu, R. K. Boyapati, N. A. Kennedy, D. A. Dorward, C. L. Noble, T. Shimizu, R. N. Carter, E. T. S. Chew, N. M. Morton, A. G. Rossi, R. B. Sartor, J. P. Iredale, J. Satsangi, MDR1 deficiency impairs mitochondrial homeostasis and promotes intestinal inflammation. *Mucosal Immunol.* **11**, 120–130 (2018).
8. D. N. Jackson, M. Panopoulos, W. L. Neumann, K. Turner, B. L. Cantarel, L. Thompson-Snipes, T. Dassopoulos, L. A. Feagins, R. F. Souza, J. C. Mills, R. S. Blumberg, K. Venuprasad, W. E. Thompson, A. L. Theiss, Mitochondrial dysfunction during loss of prohibitin 1 triggers Paneth cell defects and ileitis. *Gut* **69**, 1928–1938 (2020).
9. S. Khaloian, E. Rath, N. Hammoudi, E. Gleisinger, A. Blutke, P. Giesbertz, E. Berger, A. Metwaly, N. Waldschmitt, M. Allez, D. Haller, Mitochondrial impairment drives intestinal stem cell transition into dysfunctional Paneth cells predicting Crohn's disease recurrence. *Gut* **69**, 1939–1951 (2020).
10. R. K. Boyapati, D. A. Dorward, A. Tamborska, R. Kalla, N. T. Ventham, M. K. Doherty, P. D. Whitfield, M. Gray, J. Loane, A. G. Rossi, J. Satsangi, G.-T. Ho, Mitochondrial DNA is a pro-inflammatory damage-associated molecular pattern released during active IBD. *Inflamm. Bowel Dis.* **24**, 2113–2122 (2018).
11. E. Rath, E. Berger, A. Messlik, T. Nunes, B. Liu, S. C. Kim, N. Hoogenraad, M. Sans, R. B. Sartor, D. Haller, Induction of dsRNA-activated protein kinase links mitochondrial unfolded protein response to the pathogenesis of intestinal inflammation. *Gut* **61**, 1269–1278 (2012).
12. S. Gao, J. Hu, Mitochondrial fusion: The machineries in and out. *Trends Cell Biol.* **31**, 62–74 (2021).
13. R. Quintana-Cabrera, L. Scorrano, Determinants and outcomes of mitochondrial dynamics. *Mol. Cell* **83**, 857–876 (2023).
14. J. van Horssen, P. van Schaik, M. Witte, Inflammation and mitochondrial dysfunction: A vicious circle in neurodegenerative disorders? *Neurosci. Lett.* **710**, 132931 (2019).

15. Y.-H. Chiu, S.-C. A. Lin, C.-H. Kuo, C.-J. Li, Molecular machinery and pathophysiology of mitochondrial dynamics. *Front. Cell Dev. Biol.* **9**, 743892 (2021).
16. D. C. Chan, Mitochondrial dynamics and its involvement in disease. *Annu. Rev. Pathol.* **15**, 235–259 (2020).
17. A. Irazoki, I. Gordaliza-Alaguero, E. Frank, N. N. Giakoumakis, J. Seco, M. Palacín, A. Gumà, L. Sylow, D. Sebastián, A. Zorzano, Disruption of mitochondrial dynamics triggers muscle inflammation through interorganellar contacts and mitochondrial DNA mislocation. *Nat. Commun.* **14**, 108 (2023).
18. A. Rodríguez-Nuevo, A. Díaz-Ramos, E. Noguera, F. Díaz-Sáez, X. Duran, J. P. Muñoz, M. Romero, N. Plana, D. Sebastián, C. Tezze, V. Romanello, F. Ribas, J. Seco, E. Planet, S. R. Doctrow, J. González, M. Borrás, M. Liesa, M. Palacín, J. Vendrell, F. Villarroja, M. Sandri, O. Shirihai, A. Zorzano, Mitochondrial DNA and TLR9 drive muscle inflammation upon Opa1 deficiency. *EMBO J.* **37**, e96553 (2018).
19. R. J. Youle, A. M. van der Bliek, Mitochondrial fission, fusion, and stress. *Science* **337**, 1062–1065 (2012).
20. J. Bereiter-Hahn, M. Voth, Dynamics of mitochondria in living cells: Shape changes, dislocations, fusion, and fission of mitochondria. *Microsc. Res. Tech.* **27**, 198–219 (1994).
21. Y. Haberman, R. Karns, P. J. Dexheimer, M. Schirmer, J. Somekh, I. Jurickova, T. Braun, E. Novak, L. Bauman, M. H. Collins, A. Mo, M. J. Rosen, E. Bonkowski, N. Gotman, A. Marquis, M. Nistel, P. A. Rufo, S. S. Baker, C. G. Sauer, J. Markowitz, M. D. Pfefferkorn, J. R. Rosh, B. M. Boyle, D. R. Mack, R. N. Baldassano, S. Shah, N. S. Leleiko, M. B. Heyman, A. M. Griffiths, A. S. Patel, J. D. Noe, B. J. Aronow, S. Kugathasan, T. D. Walters, G. Gibson, S. D. Thomas, K. Mollen, S. Shen-Orr, C. Huttenhower, R. J. Xavier, J. S. Hyams, L. A. Denson, Ulcerative colitis mucosal transcriptomes reveal mitochondriopathy and personalized mechanisms underlying disease severity and treatment response. *Nat. Commun.* **10**, 38 (2019).
22. C. S. Smillie, M. Biton, J. Ordovas-Montanes, K. M. Sullivan, G. Burgin, D. B. Graham, R. H. Herbst, N. Rogel, M. Slyper, J. Waldman, M. Sud, E. Andrews, G. Velonias, A. L. Haber, K. Jagadeesh, S. Vickovic, J. Yao, C. Stevens, D. Dionne, L. T. Nguyen, A.-C. Villani, M. Hofree, E. A. Creasey, H. Huang, O. Rozenblatt-Rosen, J. J. Garber, H. Khalili, A. N. Desch, M. J. Daly, A. N. Ananthakrishnan, A. K. Shalek, R. J. Xavier, A. Regev, Intra- and inter-cellular rewiring of the human colon during ulcerative colitis. *Cell* **178**, 714–730.e22 (2019).
23. J. Lloyd-Price, C. Arze, A. N. Ananthakrishnan, M. Schirmer, J. Avila-Pacheco, T. W. Poon, E. Andrews, N. J. Ajami, K. S. Bonham, C. J. Brislawn, D. Casero, H. Courtney, A. Gonzalez, T. G. Graeber, A. B. Hall, K. Lake, C. J. Landers, H. Mallick, D. R. Plichta, M. Prasad, G. Rahnavard, J. Sauk, D. Shungin, Y. Vázquez-Baeza, R. A. White III, IBDMDB Investigators, J. Braun, L. A. Denson, J. K. Jansson, R. Knight, S. Kugathasan, D. P. B. McGovern, J. F. Petrosino, T. S. Stappenbeck, A. S. Winter, C. B. Clish, E. A. Franzosa, H. Vlamakis, R. J. Xavier, C. Huttenhower, Multi-omics of the gut microbial ecosystem in inflammatory bowel diseases. *Nature* **569**, 655–662 (2019).
24. E. R. Mann, Y. K. Lam, H. H. Uhlig, Short-chain fatty acids: Linking diet, the microbiome and immunity. *Nat. Rev. Immunol.* **24**, 577–595 (2024).
25. G. Hudson, P. Amati-Bonneau, E. L. Blakely, J. D. Stewart, L. He, A. M. Schaefer, P. G. Griffiths, K. Ahlqvist, A. Suomalainen, P. Reynier, R. M. Farland, D. M. Turnbull, P. F. Chinnery, R. W. Taylor, Mutation of OPA1 causes dominant optic atrophy with external ophthalmoplegia, ataxia, deafness and multiple mitochondrial DNA deletions: A novel disorder of mtDNA maintenance. *Brain* **131**, 329–337 (2008).
26. D. M. McKay, N. L. Mancini, J. Shearer, T. Shutt, Perturbed mitochondrial dynamics, an emerging aspect of epithelial-microbe interactions. *Am. J. Physiol. Gastrointest. Liver Physiol.* **318**, G748–G762 (2020).
27. H.-G. Sprenger, T. Langer, The good and the bad of mitochondrial breakups. *Trends Cell Biol.* **29**, 888–900 (2019).
28. K. M. Alula, D. N. Jackson, A. D. Smith, D. S. Kim, K. Turner, E. Odstrcil, B. A. Kaiparettu, T. Dassopoulos, K. Venuprasad, L. A. Feagins, A. L. Theiss, Targeting mitochondrial damage as a therapeutic for ileal Crohn's disease. *Cells* **10**, 1349 (2021).
29. A. K. Müller-Rischart, A. Pils, P. Beaudette, M. Patra, K. Hadian, M. Funke, R. Peis, A. Deleinlein, C. Schweimer, P.-H. Kuhn, S. F. Lichtenthaler, E. Motori, S. Hrelia, W. Wurst, D. Trümbach, T. Langer, D. Krappmann, G. Dittmar, J. Tatzelt, K. F. Winkhofer, The E3 ligase parkin maintains mitochondrial integrity by increasing linear ubiquitination of NEMO. *Mol. Cell* **49**, 908–921 (2013).
30. Z. Liu, J. Lei, T. Wu, W. Hu, M. Zheng, Y. Wang, J. Song, H. Ruan, L. Xu, T. Ren, W. Xu, Z. Wen, Lipogenesis promotes mitochondrial fusion and maintains cancer stemness in human NSCLC. *JCI Insight* **8**, e158429 (2023).
31. T. MacVicar, T. Langer, OPA1 processing in cell death and disease—The long and short of it. *J. Cell Sci.* **129**, 2297–2306 (2016).
32. A. Olichon, E. Guillou, C. Delettre, T. Landes, L. Arnauné-Pelloquin, L. J. Emorine, V. Mills, M. Daloyau, C. Hamel, P. Amati-Bonneau, D. Bonneau, P. Reynier, G. Lenaers, P. Belenguer, Mitochondrial dynamics and disease, OPA1. *Biochim. Biophys. Acta* **1763**, 500–509 (2006).
33. Z. Song, H. Chen, M. Fiket, C. Alexander, D. C. Chan, OPA1 processing controls mitochondrial fusion and is regulated by mRNA splicing, membrane potential, and Yme1L. *J. Cell Biol.* **178**, 749–755 (2007).
34. T. Wai, J. García-Prieto, M. J. Baker, C. Merkwirth, P. Benit, P. Rustin, F. J. Rupérez, C. Barbas, B. Ibañez, T. Langer, Imbalanced OPA1 processing and mitochondrial fragmentation cause heart failure in mice. *Science* **350**, aad0116 (2015).
35. B. Head, L. Griparic, M. Amiri, S. Gandre-Babbe, A. M. van der Bliek, Inducible proteolytic inactivation of OPA1 mediated by the OMA1 protease in mammalian cells. *J. Cell Biol.* **187**, 959–966 (2009).
36. N. L. Mancini, L. Goudie, W. Xu, R. Sabouny, S. Rajeev, A. Wang, N. Esquerre, A. A. Rajabi, T. S. Jayme, E. van Tilburg Bernardes, Y. Nasser, J. G. P. Ferraz, T. Shutt, J. Shearer, D. M. McKay, Perturbed mitochondrial dynamics is a novel feature of colitis that can be targeted to lessen disease. *Cell. Mol. Gastroenterol. Hepatol.* **10**, 287–307 (2020).
37. A. Dashdorj, K. R. Jyothi, S. Lim, A. Jo, M. N. Nguyen, J. Ha, K.-S. Yoon, H. J. Kim, J.-H. Park, M. P. Murphy, S. S. Kim, Mitochondria-targeted antioxidant MitoQ ameliorates experimental mouse colitis by suppressing NLRP3 inflammasome-mediated inflammatory cytokines. *BMC Med.* **11**, 178 (2013).
38. A. Wang, Á. V. Keita, V. Phan, C. M. McKay, I. Schoutz, J. Lee, M. P. Murphy, M. Fernando, N. Ronaghan, D. Balce, R. Yates, M. Dickey, P. L. Beck, W. K. M. Naughton, J. D. Söderholm, D. M. McKay, Targeting mitochondria-derived reactive oxygen species to reduce epithelial barrier dysfunction and colitis. *Am. J. Pathol.* **184**, 2516–2527 (2014).
39. F. M. Yakes, B. Van Houten, Mitochondrial DNA damage is more extensive and persists longer than nuclear DNA damage in human cells following oxidative stress. *Proc. Natl. Acad. Sci. U.S.A.* **94**, 514–519 (1997).
40. N. M. Druzhyna, G. L. Wilson, S. P. LeDoux, Mitochondrial DNA repair in aging and disease. *Mech. Ageing Dev.* **129**, 383–390 (2008).
41. K. Nakada, K. Inoue, T. Ono, K. Isobe, A. Ogura, Y. I. Goto, I. Nonaka, J. I. Hayashi, Inter-mitochondrial complementation: Mitochondria-specific system preventing mice from expression of disease phenotypes by mutant mtDNA. *Nat. Med.* **7**, 934–940 (2001).
42. T. Ono, K. Isobe, K. Nakada, J.-I. Hayashi, Human cells are protected from mitochondrial dysfunction by complementation of DNA products in fused mitochondria. *Nat. Genet.* **28**, 272–275 (2001).
43. W. Y. Yang, Optogenetic probing of mitochondrial damage responses. *Ann. N. Y. Acad. Sci.* **1350**, 48–51 (2015).
44. J. B. Stewart, P. F. Chinnery, The dynamics of mitochondrial DNA heteroplasmy: Implications for human health and disease. *Nat. Rev. Genet.* **16**, 530–542 (2015).
45. K. Lewis, F. Lutgendorff, V. Phan, J. D. Söderholm, P. M. Sherman, D. M. McKay, Enhanced translocation of bacteria across metabolically stressed epithelia is reduced by butyrate. *Inflamm. Bowel Dis.* **16**, 1138–1148 (2010).
46. K. E. Cunningham, G. Vincent, C. P. Sodhi, E. A. Novak, S. Ranganathan, C. E. Egan, D. B. Stolz, M. B. Rogers, B. Firek, M. J. Morowitz, G. K. Gittes, B. S. Zuckerbraun, D. J. Hackam, K. P. Mollen, Peroxisome proliferator-activated receptor- $\gamma$  coactivator 1- $\alpha$  (PGC1 $\alpha$ ) protects against experimental murine colitis. *J. Biol. Chem.* **291**, 10184–10200 (2016).
47. K. Takahashi, A. Nishida, T. Fujimoto, M. Fujii, M. Shioya, H. Imaeda, O. Inatomi, S. Bamba, M. Sugimoto, A. Andoh, Reduced abundance of butyrate-producing bacteria species in the fecal microbial community in Crohn's disease. *Digestion* **93**, 59–65 (2016).
48. H. C. Clevers, C. L. Bevins, Paneth cells: Maestros of the small intestinal crypts. *Annu. Rev. Physiol.* **75**, 289–311 (2013).
49. C. Becker, M. C. Fantini, S. Wirtz, A. Nikolaev, R. Kiesslich, H. A. Lehr, P. R. Galle, M. F. Neurath, In vivo imaging of colitis and colon cancer development in mice using high resolution chromoendoscopy. *Gut* **54**, 950–954 (2005).
50. S. Wirtz, V. Popp, M. Kindermann, K. Gerlach, B. Weigmann, S. Fichtner-Feigl, M. F. Neurath, Chemically induced mouse models of acute and chronic intestinal inflammation. *Nat. Protoc.* **12**, 1295–1309 (2017).
51. M. Leppkes, C. Becker, I. I. Ivanov, S. Hirth, S. Wirtz, C. Neufert, S. Pouly, A. J. Murphy, D. M. Valenzuela, G. D. Yancopoulos, B. Becher, D. R. Littman, M. F. Neurath, ROR $\gamma$ -expressing Th17 cells induce murine chronic intestinal inflammation via redundant effects of IL-17A and IL-17F. *Gastroenterology* **136**, 257–267 (2009).
52. T. Sato, R. G. Vries, H. J. Snippert, M. van de Wetering, N. Barker, D. E. Stange, J. H. van Es, A. Abo, P. Kujala, P. J. Peters, H. Clevers, Single Lgr5 stem cells build crypt-villus structures in vitro without a mesenchymal niche. *Nature* **459**, 262–265 (2009).
53. M. Bardenbacher, B. Ruder, N. Britzen-Laurent, E. Naschberger, C. Becker, R. Palmisano, M. Stürzl, P. Tripal, Investigating intestinal barrier breakdown in living organoids. *J. Vis. Exp.* **157**, e60546 (2020).
54. C. Becker, S. Wirtz, M. Blessing, J. Pirhonen, D. Strand, O. Bechthold, J. Frick, P. R. Galle, I. Autenrieth, M. F. Neurath, Constitutive p40 promoter activation and IL-23 production in the terminal ileum mediated by dendritic cells. *J. Clin. Invest.* **112**, 693–706 (2003).
55. B. Kircher, S. Woltemate, F. Gutzki, D. Schlüter, R. Geffers, H. Bähre, M. Vital, Predicting butyrate- and propionate-forming bacteria of gut microbiota from sequencing data. *Gut Microbes* **14**, 2149019 (2022).

**Acknowledgments:** The microbiome analysis was supported by the Microbiome Analysis Center Erlangen (MACE). We thank E. Liebing for critical proofreading and V. Thonn, E. Podstawa, and N. Gießl for excellent technical assistance. Parts of the results of this study are a

subject of the doctoral thesis of L.-L.B. **Funding:** This work was funded by the Deutsche Forschungsgemeinschaft (DFG) projects 375876048 (TRR241 projects A03 to C.B. and S.W., A06 to M.S., A08 to K.H., B01 to B.S., B05 to J.V.P., B06 to S.M.K., C02 to R.A., C04 to M.F.N., Z02 to C.B. and B.S., and Z03 to Z.T., A.K., and R.A.) and 261193037 (SFB1181 projects C02 to M.F.N. and C05 to M.F.N.) and individual grants with the project numbers 418055832 and 510624836 to C.B. The project was also supported by the Interdisciplinary Centre for Clinical Research (IZKF: A76 and A93 to C.B.). Super-resolution spinning disk microscopy was enabled on an EVIDENT Spinning Disc, funded by DFG-project 522417173 to the OICE. **Author contributions:** Study concept, literature search, experimentation, analysis, interpretation of data, and critical revision of manuscript were performed by C.B., Y.-Q.Y., L.-L.B., Z.T., G.S., M.S., A.G., and J.V.P. Experimentation and analysis were performed by L.-L.B., M.G.-A., S.M.K., B.S., P.T., L.E., R.G.-B., M.M.A., S.W., and Z.T. Material support was provided by R.A., A.Z., K.H., A.A.K., and M.T.C. Manuscript drafting was prepared by L.-L.B. and C.B. Intellectual contributions, manuscript editing, and material support were performed by L.-L.B., C.B., M.F.N., A.Z., B.S., and J.V.P. **Competing interests:** B.S. consulted for AbbVie, Abivax, Boehringer Ingelheim, Bristol Myers Squibb, Dr. Falk Pharma, Eli Lilly, Endpoint Health, Falk, Galapagos, Gilead, Janssen, Landos, Lilly, Materia Prima, PredictImmune, Pfizer, and Takeda. B.S. received speaker fees from AbbVie, AlfaSigma, BMS, CED Service GmbH, Dr. Falk Pharma, Eli Lilly, MSD, Ferring, Galapagos, Janssen, Pfizer, and Takeda. B.S. received a grant from Pfizer. M.F.N. consulted for AbbVie, Boehringer Ingelheim, Dr. Falk Pharma, PPM, Eli Lilly, Pentax, Dr. Falk Pharma, Gilead, Janssen, NovoNordisc Foundation, Lilly, Pfizer, and Takeda. M.F.N. received speaker fees from AbbVie, BMS, Dr. Falk Pharma, Eli Lilly, Ferring, Janssen, Pfizer, and Takeda. M.F.N. received a grant from PPM. The other authors declare that they have no competing interests. **Data and materials availability:** All data associated with this study are present in the paper or the Supplementary Materials. GEO-ID of PROTECT cohort data of patients with UC: GSE109142. Transcriptomic data from the IBDome cohort (v0.50) are available at <https://ibdome.org>. Transcriptomic data from mouse *Opa1* KO tissues and organoids have been uploaded to the European Nucleotide Archive through ArrayExpress (<https://ebi.ac.uk/biostudies/arrayexpress>) under accession numbers E-MTAB-14487 and E-MTAB-14488, respectively. Microbiome sequencing data from the mouse *Opa1* KO stool have been deposited at the European Nucleotide Archive under the project number PRJEB83275. The RNA-seq data of DSS time-course experiments have been uploaded to the European nucleotide archive through ArrayExpress (<https://ebi.ac.uk/biostudies/arrayexpress>) under accession number E-MTAB-9850. Publicly available single-cell data can be accessed in Single Cell Portal ([https://singlecell.broadinstitute.org/single\\_cell/study/SCP259/](https://singlecell.broadinstitute.org/single_cell/study/SCP259/)).

The 3D visualization of the mitochondrial length was performed using a macro code (<https://doi.org/10.5281/zenodo.14287796>). OPA1-deficient mice can be provided under a material transfer agreement.

**The TRR241 IBDome Consortium:** In addition to the TRR241 IBDome Consortium members who are authors (R.A., C.B., K.H., S.K., A.A.K., M.N., J.V.P., B.S., M.S., S.W., and Z.T.), the following TRR241 IBDome Consortium members are collaborators who have contributed to either study design, sample collection, data analysis, and/or interpretation: Imke Atreya<sup>1</sup>, Petra Bacher<sup>2,3</sup>, Christian Bojarski<sup>4</sup>, Nathalie Britzen-Laurent<sup>1</sup>, Caroline Bosch-Voskens<sup>1</sup>, Hyun-Dong Chang<sup>5</sup>, Andreas Diefenbach<sup>6</sup>, Claudia Günther<sup>1</sup>, Ahmed N. Hegazy<sup>4</sup>, Christoph S. N. Klose<sup>6</sup>, Kristina Koop<sup>1</sup>, Moritz Leppkes<sup>1</sup>, Rocio López-Posadas<sup>1</sup>, Leif S.-H. Ludwig<sup>7</sup>, Clemens Neufert<sup>1</sup>, Christina Plattner<sup>9</sup>, Magdalena Prüß<sup>3</sup>, Andreas Radbruch<sup>5</sup>, Chiara Romagnani<sup>3</sup>, Francesca Ronchi<sup>6</sup>, Ashley Sanders<sup>4,8</sup>, Alexander Scheffold<sup>2</sup>, Jörg-Dieter Schulzke<sup>4</sup>, Michael Schumann<sup>4</sup>, Sebastian Schürmann<sup>1</sup>, Antigoni Triantafyllou<sup>5,10</sup>, Maximilian Waldner<sup>1</sup>, Carl Weidinger<sup>4</sup>, Sebastian Zundler<sup>1</sup>.

Affiliations 1, 4, and 9 can be found on the first page of the paper. <sup>2</sup>Institute of Clinical Molecular Biology, Christian-Albrecht University of Kiel, Kiel, Germany. <sup>3</sup>Institute of Immunology, Christian-Albrecht University of Kiel and UKSH Schleswig-Holstein, Kiel, Germany. <sup>5</sup>Deutsches Rheuma-Forschungszentrum, ein Institut der Leibniz-Gemeinschaft, Berlin, Germany. <sup>6</sup>Institute of Microbiology, Infectious Diseases and Immunology, Charité–Universitätsmedizin Berlin, corporate member of Freie Universität Berlin and Humboldt-Universität zu Berlin, Berlin, Germany. <sup>7</sup>Berlin Institut für Gesundheitsforschung, Medizinische System Biologie, Charité–Universitätsmedizin Berlin, Berlin, Germany. <sup>8</sup>Max Delbrück Center für Molekulare Medizin, Charité–Universitätsmedizin Berlin, Berlin, Germany. <sup>10</sup>Department of Rheumatology and Clinical Immunology, Charité–Universitätsmedizin Berlin, corporate member of Freie Universität Berlin and Humboldt-Universität zu Berlin, Berlin, Germany.

Submitted 4 January 2024

Resubmitted 1 October 2024

Accepted 18 December 2024

Published 15 January 2025

10.1126/scitranslmed.adn8699